Journal of Magnetic Resonance 294 (2018) 16–23

Contents lists available at ScienceDirect

Journal of Magnetic Resonance

journal homepage: www.elsevier.com/locate/jmr

Revealing how interfaces in stacked thin fibrous layers affect liquid ingress and transport properties by single-sided NMR

Behzad Mohebbi [a,b,*], Amir Hossein Tavangarrad [c], Jan Claussen [b], Bernhard Blümich [a], S. Majid Hassanizadeh [c], Rodrigo Rosati [b]

[a] Institute for Technical and Macromolecular Chemistry, Worringerweg 2, RWTH Aachen University, 52056 Aachen, Germany
[b] Procter&Gamble Service GmbH, Sulzbacher Str. 40, 65824 Schwalbach am Taunus, Germany
[c] Department of Earth Sciences, Environmental Hydrogeology Group, Utrecht University, Princetonplein 9, 3584CC Utrecht, The Netherlands

ARTICLE INFO

Article history:
Received 18 December 2017
Revised 22 June 2018
Accepted 23 June 2018
Available online 25 June 2018

Keywords:
Thin porous media
Single-sided NMR
PEM fuel cell
Fluid flow visualization

ABSTRACT

Offering multifaceted applications, thin fibrous porous materials are mostly used in stacks of layers, each layer having a defined functionality. Since only a few pores exist across a layer a couple of hundred microns thick, the interface between layers may significantly affect liquid ingress. Thus, the main objective of the study is to substantiate that an interface layer is present during liquid infiltration between stacked thin fibrous layers and that it affects the fluid transport properties. A compact single-sided NMR device with a low static gradient of about 2 T/m perpendicular to the sensor surface and a uniform magnetic field in lateral directions was used to profile a 2-mm thick slice in one shot. The liquid ingress into the thin fibrous layers and their interfaces was visualized by Fourier-transforming the NMR signal and processing the time-dependent 1D profiles with a newly developed mathematical method. The flow characteristics and liquid distribution profiles of a 400-μm thick layer were compared with those of two stacked 200-μm thick layers from the same material but with an interface between them. The results show major differences in distributions and flow dynamics for the single and dual layer cases, which reveal the importance of the interface in fluid flow.

1. Introduction

Thin nonwoven fibrous materials boast a wide range of applications in various products such as papers, filters, fuel cells, fluid absorbents or barrier materials, textiles, diapers, and pads. A thin porous layer is defined by a thickness that is orders of magnitude lower than its lateral dimensions. An apt example of such a layer is the gas-diffusion layer (GDL) in proton-exchange membrane fuel cells with a thickness of about 200 μm, three orders of magnitude smaller than its lateral dimensions. Pointing to the few pores along the layer thickness, Ceballos et al. [1] distinguished this layer as a network of interconnected capillaries. However, thin porous layers behave differently from thick porous media: It has been shown that some of the physical phenomena, which are negligible in thick porous media, play a dominant role in a thin porous medium [2].

Thin porous media pose a number of research questions that theoretical, numerical, and experimental techniques have aimed to address [2]. The flow of liquids through a stack of thin porous layers under unsaturated conditions is one of the important processes to be considered. Often these layers have different properties. For example, the previously mentioned GDL layer is next to another layer known as microporous layer (MPL) [3,4]. Moreover, several layers with different functionalities are employed in diapers, for instance [5]. Another example is coated paper used in inkjet printing. Even though the interfaces generated between thin porous layers play an important role in the unsaturated fluid flow only few numerical and experimental studies have dealt with interfaces in thin fibrous layers. In numerical studies, one approach to model the stacked thin porous layers and their interface is to simulate the interface between two adjacent layers as a third virtual layer [2].For this approach, the study of transport phenomena at the interface of two porous media or a porous medium and a free fluid could be useful [6,7]. Another approach is to simulate the layers as two-dimensional continua and include the interface pressure in exchange of mass between the layers [8,9].

Experimental studies of fluid distributions and their dynamics inside thin layers and their interfaces are a challenging task. There are different non-destructive techniques, such as X-ray tomography [10], confocal microscopy, and scanning neutron radiology [11], which have been employed to investigate the transport and

* Corresponding author at: Institute for Technical and Macromolecular Chemistry, Worringerweg 2, RWTH Aachen University, 52056 Aachen, Germany.
E-mail address: mohebbi.b@pg.com (B. Mohebbi).

https://doi.org/10.1016/j.jmr.2018.06.014
1090-7807/

distribution of water within porous substrates. However, benchtop setups for such measurements are challenging. In addition, magnetic resonance imaging (MRI) enables noninvasive monitoring of fluid flow through porous materials. In the literature, MRI has been reported for determining moisture content in textile and fibrous materials such as carpets [12] filtration materials [13,14] and papers [15,16]. Although the drying process across the thickness as well as the fluid transport such as wicking have been investigated in these studies [17], the effect of the interface region between the porous layers was not studied. Whereas MRI may provide very detailed information, it is often associated with high effort needed for the post-processing of the data.

Alternatively, mobile single-sided nuclear magnetic resonance (NMR) has been used for determining liquid distributions inside porous materials, such as soil, concrete, building materials and food [18–20]. Although, the open geometry of these NMR sensors results in inhomogeneous magnetic measurement and radio-frequency fields B_0 and B_1, respectively, sub-millimeter depth resolution can be achieved with sensors providing a time-invariant gradient G_0 perpendicular to the magnet surface. The depth resolution can be optimized by minimizing the ratio $\Delta B/G_0$, where ΔB is the magnetic field variation in the lateral directions perpendicular to the gradient direction.

The Profile NMR-MOUSE is an example of such a sensor which provides resolutions better than 10 μm due to very low lateral-field variation at a particular distance from the sensor surface, where the magnetic field gradient is about 20 T/m [21]. This high gradient poses an upper limit of about 100 μm for the thickness of the slice that can be excited, because of the finite bandwidth of the transmit/receive circuit. Therefore, the system needs to be precisely positioned and repositioned to measure profiles over a few millimeters. In order to better understand the dynamic effect of the interface on liquid flow, it is important to excite not only the interface area but the whole assembly of several layers and their interfaces. This cannot be captured using this standard approach.

To solve this problem, it is necessary to excite a thicker slice that covers several layers across a range of a few millimeters. This can be done by reducing the quality factor of the rf circuit to excite a broader bandwidth [22] at the expense of lowering the detection sensitivity. Alternatively the thickness of the excited slice can be increased by decreasing the magnetic field gradient of the sensor. Following this approach, 8-mm thick profiles have been measured with a resolution of 200 μm [23]. However, this resolution does not suffice to resolve the phenomena at interfaces of thin porous layers with thickness in the same range.

In this work, a low-gradient single-sided NMR-MOUSE prototype, known as *Fourier NMR-MOUSE,* has been employed. This sensor exhibits a 10-fold lower gradient in the depth direction than the Profile NMR-MOUSE across the width of the sensitive slice, thanks to a sophisticated arrangement of magnets. This sensor exhibits a gradient of about 2 T/m so that a 2-mm thick slice can be scanned in one shot with a depth resolution of about 25 μm [24].

The principal objective of this current study is to provide evidence that an interface layer is indeed present during liquid infiltration between stacked thin fibrous layers and that this interface affects the fluid transport properties. Consequently, a novel experimental procedure is elaborated for the Fourier NMR-MOUSE to investigate the effect of the interface on fluid flow through thin fibrous porous layers. The signal is acquired with a CPMG sequence. The acquired data are Fourier-transformed to obtain the signal intensity over time and position. To correct for amplitude distortions resulting from the inhomogeneous magnetic field in the depth direction, the signal amplitude of the thin porous layer during fluid injection with a constant flow rate was normalized to the signal intensity of bulk liquid as a mask function.

2. Experimental method

2.1. The Fourier NMR-MOUSE

The sensor used in this work consists of a main unit, a U-shaped magnet, and a shim unit with four movable smaller magnets. This unit generates the main magnetic field, and the shim unit is used to adjust the stray magnetic field in such a way that the gradient in the depth direction is reduced while the field strength in the lateral direction, i.e. the direction parallel to the sensor surface remains essentially constant across the width of the sensitive volume [24]. The resultant field strength of the sensor is 0.2 T corresponding to 8.5 MHz for hydrogen nuclei, and the static gradient of 1.87 T/m in the depth direction enables excitation of a 2-mm thick slice.

2.2. Materials

In order to investigate the effect of the interface, two spunbonded fibrous layers produced in the same way and from the same material, but differing only in their areal density and, thus, in their thickness, were stacked for measurement. With this setup, other effects arising from the interaction of layers with different structures and properties were avoided. The non-woven layers used in this study were made of polyethylene terephthalate fibers and chosen so that the stack of two layers has the same thickness as a layer with double the basis weight. Therefore, an 86 gsm (g/m^2) polyester fabric with a thickness of 400 μm was compared to the stack of two layers of 43 gsm polyester fabric 200 μm each. The two layers were pushed together under a pressure of 0.3 psi, and were imaged with a Keyence VHX 5000 Digital microscope. The resulting image and enlarged section are shown in Fig. 1. The gap between these layers is referred to as the "interface area" that can be distinguished from the two layers in this image. The thickness of the two 43 gsm layers was measured to be 600 ± 7 μm which includes the thickness of the two layers plus the interface in between. In order to observe the porosity change over the thickness of two stacked layers, a μCT scanner (Scanco μCT50) with 4 μm isotropic voxel resolution was used and a square sample of 4 mm by 4 mm was cut and scanned under 0.3psi pressure. The μCT images were imported to ImageJ software for thresholding and noise filtration. In the next step, the porosity over the thickness was evaluated, as shown in Fig. 2. To do this, a MATLAB code was developed in-house that uses binarized images as input. The section with higher porosity that is illustrated in Fig. 2 corresponds to the interface region between the layers. The layers were made from polyester fibers with a density of 1.38 g/cm^3, and the fibers were hydrophilized with a surfactant. These materials exhibited negligible swelling in the chosen working liquid, a saline solution consisting of 0.9% NaCl and distilled water. This solution had a surface tension of 72.5 mN/M, a density of 1.005 g/cm^3, and viscosity of 1.017 mPa s.

2.3. Experimental procedure

As already mentioned, the main objective of this study is to substantiate that an interface layer is present in between stacked thin fibrous layers and that it affects the fluid transport properties. To achieve this goal, we visualized the 1D time-resolved depth profile of the liquid flow inside thin porous layers with and without an interface by using a low-field single-sided NMR device. Therefore, the same measurements were executed for a single layer of 86 gsm basis weight and a stack of two 43-gsm layers.

For the measurements, square samples with a dimension of 10×10 mm^2 were cut. A 20-g Plexiglas cube with a hole in its center for the pump tubing was placed on top of the layers in order to

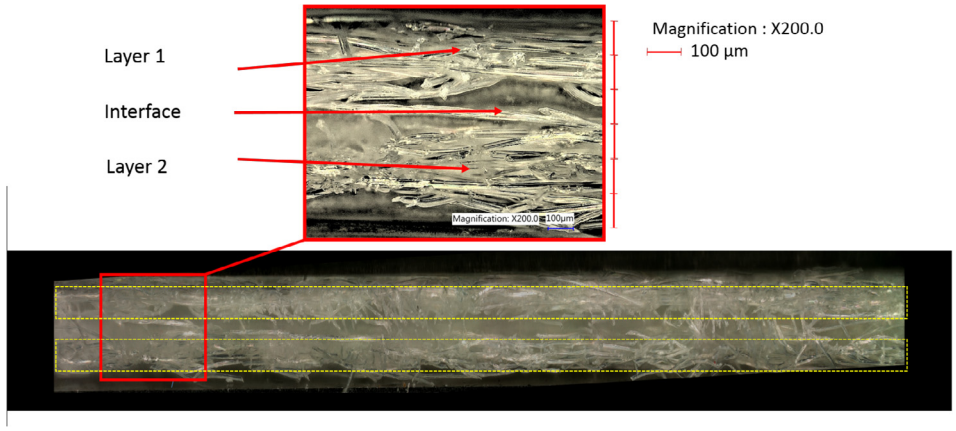

Fig. 1. Microscopy images of two 43gsm layers on top of each other after application of 0.3 psi pressure. The approximate position of each layer is marked with yellow dashed line. (For interpretation of the references to colour in this figure legend, the reader is referred to the web version of this article.)

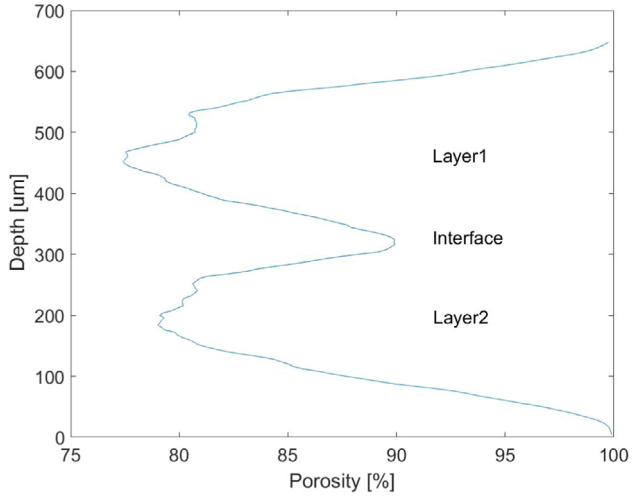

Fig. 2. Variation of fiber content over the thickness of two 43gsm layers obtained from binarized µCT images. Higher fiber content in the middle of each layer is attributed to bonding points. The lower fiber content belongs to the interface region in between two layers.

ensure the same distance between the individual layers in successive experiments. A syringe pump attached to 1-mm inner diameter tubing was used to inject the saline solution into the center of the samples at the rate of 30 µl/min (see Fig. 3). The Fourier NMR-MOUSE sensor enables us to excite the full thickness of the multilayer sample in each scan. Thus, liquid is not moving out of the excited volume during infiltration of liquid. This means that signal dephasing and loss of detectable magnetization is irrelevant in these experiments.

The NMR signal was collected using a CPMG pulse sequence composed of 512 echoes with an echo time of t_E = 160 µs. For each experiment, a total of 1000 scans was collected using a repetition time of 200 ms.

3. Data processing and normalization

3.1. Normalization process

Since the excited sensitive slice in single-sided NMR sensors does not have sharp edges, the signal amplitude in the boundaries of the excited slice is less than the amplitude in the slice center. This becomes more predominant upon investigating the fluid distribution in thin layers where the thickness of the sensitive slice is similar to the thickness of the porous layer or where the aim is to compare saturation in the boundaries and the interface of such layers.

To address this issue, the acquired data were post-processed by normalizing the image of the thin porous layer to the image (*Mask*) of bulk fluid. The signal (FT_{norm}) obtained from a CPMG echo train by Fourier Transformation (FT) and normalization are calculated according to:

$$Mask_{\mathrm{Avg}}[1,j] = \frac{\sum_i Mask[i,j]}{n}, \tag{1}$$

$$FT_{\mathrm{norm}}[i,j] = \frac{FT[i,j]}{Mask_{\mathrm{Avg}}[1,j]}, \tag{2}$$

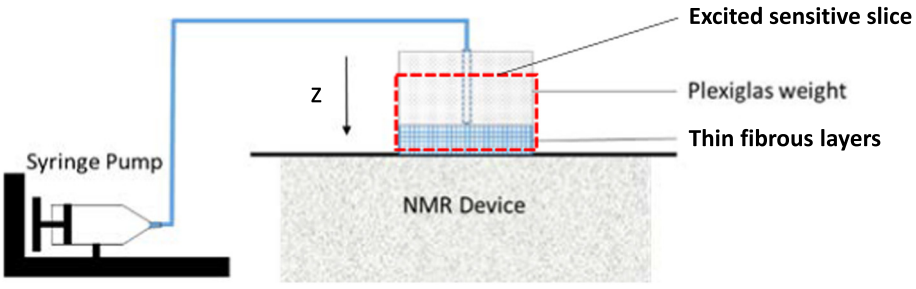

Fig. 3. Sketch of the experimental setup. The liquid is injected in the center of 10 × 10 mm^2 samples with a syringe pump. For the 43 gsm sample, two layers were placed on top of each other. A 20 g (about 0.3 psi pressure) Plexiglas weight is placed on top of the samples to ensure a constant spacing between the layers. The thickness of the excited slice is 2 mm and therefore it covers all the fibrous layers.

where *Mask* [*i,j*] denotes the time space encoding matrix of the bulk liquid, *n* is the number of scans, *i* scales time, *j* scales position in space, *FT* [*i,j*] is the matrix of original data after Fourier transformation, and FT_{norm} [*i,j*] is the normalized matrix. Fig. 4 illustrates the 1D depth profile of a 150 μm thin layer as a function of time before and after normalization and the mask function used for the normalization. The 1D depth profiles were measured with an NMR-MOUSE with a static gradient of 35 T/m. The figure illustrates that without normalization, the even liquid distribution is not accurately represented and suggests that more liquid is concentrated in the middle of the layer, which is a measurement artifact. This artifact is corrected for with the post-processing step. The same procedure is applied to the 2-mm thick 1D profiles acquired with the Fourier NMR-MOUSE.

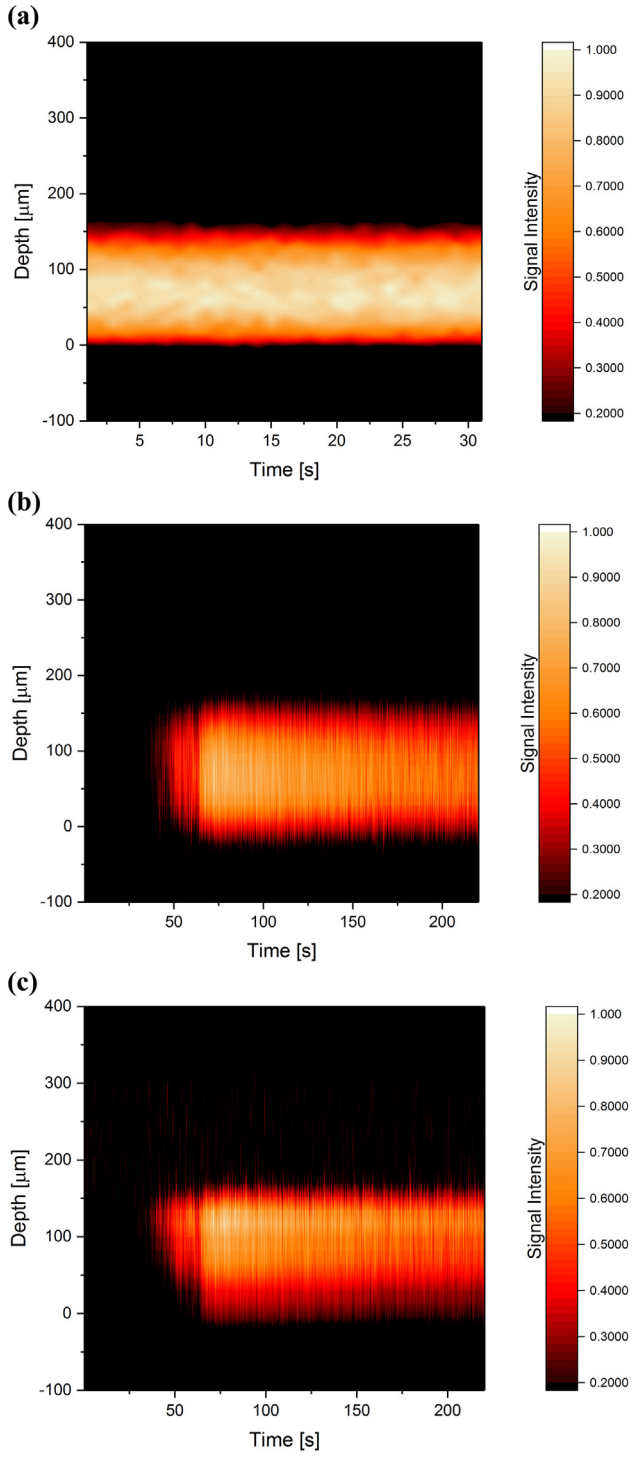

Fig. 4. Time-resolved depth profiles acquired with an NMR-MOUSE having a 150 μm-thick sensitive slice. (a) 1D depth profiles of bulk liquid. (b) 1D depth profiles of a 150 μm-thick filter paper soaked in water without normalization. (c) The same depth profiles as in (b) but after normalization and correction.

3.2. Diffusion effects

To estimate the impact of diffusion on relative signal intensity in different regions, the difference in effective diffusion coefficient inside the layer itself and in the interface area is calculated. This effective diffusion coefficient can be estimated by using equation below for fibrous materials [25]:

$$D_{eff} = D_0\ \varepsilon\left(\frac{\varepsilon-\varepsilon_p}{1-\varepsilon_p}\right)^{\alpha}, \tag{3}$$

where D_{eff} denotes the effective diffusion coefficient, D_0 is the free diffusion of the liquid, ε is the porosity, ε_p is a percolation threshold and α is an empirical constant. For fibrous porous layers, ε_p is found to be 0.11 and α is 0.785, for cross-plane diffusion. Such percolation behavior in diffusion is a typical characteristic of fibrous porous [26]. With inserting the porosity of the layer and interface obtained from Fig. 2 ($\varepsilon_{layer} \approx 0.9, \varepsilon_{interface} \approx 0.8$), the ratio of the effective diffusion inside the layer to the effective diffusion in the interface is calculated to be 0.8, i.e., equivalent to a 20% difference.

With this calculated value, the signal attenuation resulting from diffusion is determined according to:

$$I/Io = \exp\left(-\gamma^2 G^2 D t_E^2 (m t_E)\frac{2}{3}\right), \tag{4}$$

where γ denotes the gyromagnetic ratio, t_E is the echo time, *m* is the number of echoes and *G* is the static gradient. By inserting all these values into Eq. (4), the signal attenuation due to diffusion is calculated to be 2.3%. Therefore, even if we consider a 20% difference in effective diffusion to be significant, it has a minor effect on the relative signal intensity. Based on these calculations and because the goal of this current study is not to quantify the liquid amount, the effect of diffusion on the relative signal amplitude of the layer and interface area can be neglected. Again, the main goal here is to investigate the presence of an interface region during liquid infiltration in stacked thin porous layers and its effect on liquid partitioning.

3.3. Average fluid velocity

The average velocity of the fluid was approximated by taking into account the constant flow rate and dimensions of the tube and the sample for in-plane and through-plane directions, using the equations below:

$$V_{inlet,z} = Q/A = Q/\pi r^2, \tag{5}$$

$$V_{inlet,r} = Q/A = Q/2\pi rh, \tag{6}$$

$$t_T = m t_E, \tag{7}$$

$$d = V_{inlet(z,r)} \cdot t_T, \tag{8}$$

where $V_{inlet,z}$ and $V_{inlet,r}$ are the velocity in z and radial direction, respectively. The term *Q* denotes the flow rate inside the tube (30 μl/min), *h* is the layer thickness and *r* is the tube inner radius. The term d is the total distance traveled during each experiment and is calculated by Eqs. (7) and (8), where t_T is the total time of each experiment. The distance protons travel in z and radial direction is 52 μm and 66 μm, respectively. The dimensions of the sensitive

volume (2 mm in the z- and 10 mm by 10 mm in planar directions) are bigger than the distance traveled. Therefore, liquid is not moving out of the excited volume during injection of the liquid.

4. Results and discussion

Fig. 5 illustrates the time-resolved depth profiles of the 86-gsm layer and of two 43-gsm layers measured with the Fourier NMR-MOUSE. In these profiles, the difference due to the interface between two thin layers is clearly visible. In the case of the two thin layers (c, d), a narrow region with lower signal intensity, and therefore lower liquid amount, is observable in their contact interface. The thickness of the interface layer is almost in the same range as that of each of the layers. The injection of the liquid started 20 s after the recording of the profiles to identify possible signal coming from liquids remaining on the surfaces. To investigate the reproducibility of the results, each experiment was repeated. Hereby, the same results were obtained (Fig. 5a, b and c, d) apart from minor variations, which are attributed to variations in the experimental setup and in materials.

In order to study the effects of the interface on the dynamics of liquid ingress as well as the liquid distribution, depth profiles at different times and dynamic signal change in different positions were extracted from the profiles in Fig. 5. They are depicted in Figs. 6 and 7.

The development of the liquid distribution profiles over time for a single layer and a two-layer stack with an interface are shown in Fig. 6. The flow starts at t = 20 s and lasts for 60 s with a total injection volume of 30 μl. For a single fibrous layer (Fig. 6a), liquid is accumulated on top of the layer at early times. After about 50 s, liquid moves further towards the layer bottom and the signal intensity increases until it reaches an equilibrium value after about 100 s. In the case of two fibrous layers (Fig. 6b), liquid builds up mainly in the first layer during the first 30 s with no signal coming from the interface region. Once the liquid content of the first layer increases considerably, the liquid enters the interface region and the second layer at later times. It is noteworthy that there is a considerable amount of liquid in the interface region that delays the liquid ingress into the second layer. Moreover, the normalized areas below the curves are plotted versus time to check the fixed flow rate boundary condition and are shown in the inset of Fig. 6. The linearity of the areas versus time before they reach constant equilibrium values indicates constant flow rate.

In order to investigate the dynamic behavior of liquid flow into the fibrous layers and the effect of the interface between two layers, the signal amplitude over time and at different depths are exported and shown in Fig. 7. The positions are chosen inside the layers and also in the interface region based on the fully developed depth profiles. The signal amplitudes as a function of time are accordingly extracted at 100, 300 and 500 μm from the surface of

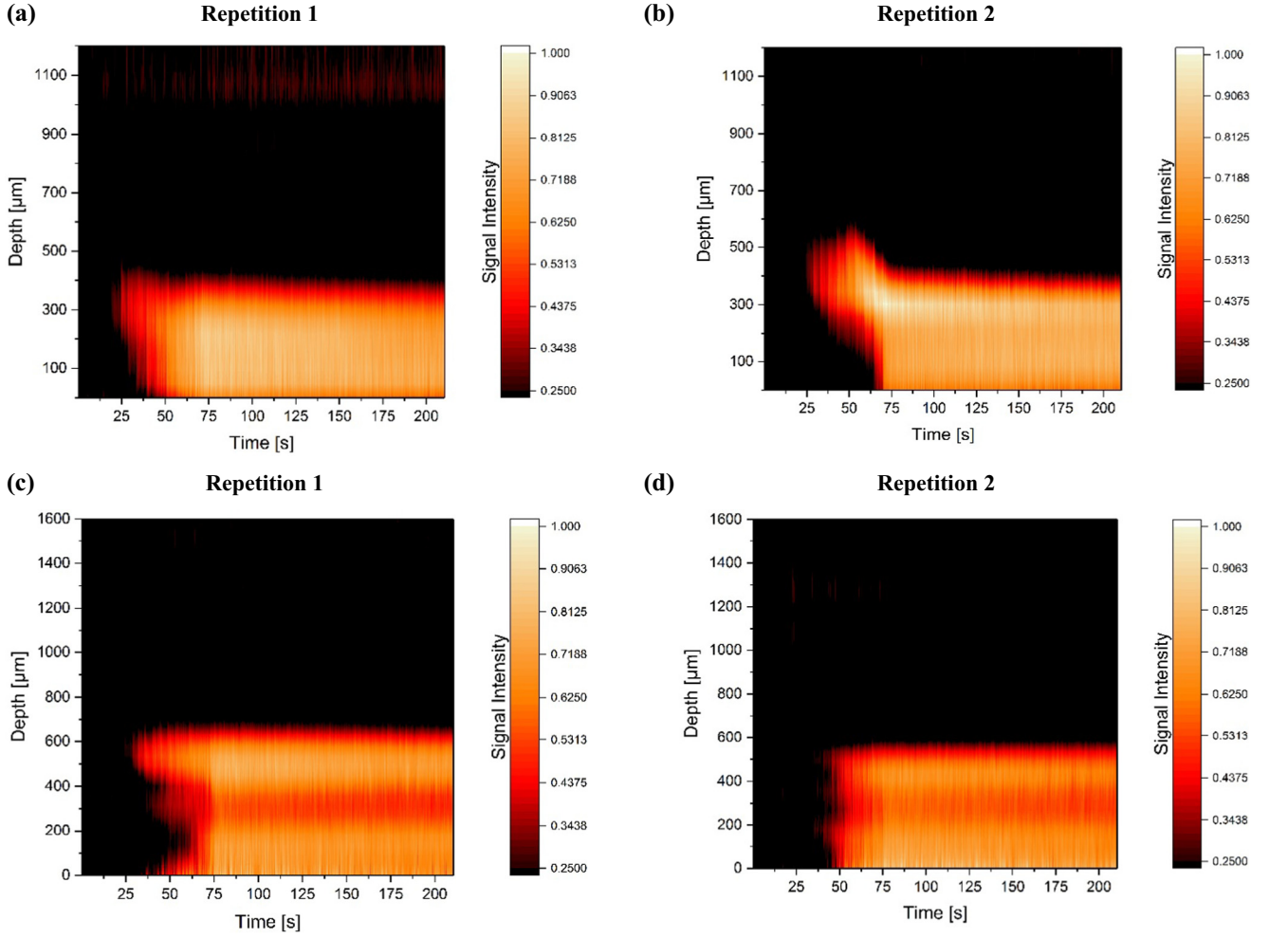

Fig. 5. The time-resolved depth profiles measured with the FOURIER NMR-MOUSE, where the zero position indicates the surface of the NMR sensor. (a, b) Two profiles of a single 86-gsm fibrous layer without interface. (c, d) Two profiles of two 43-gsm fibrous layers. The interface layer between two thin layers has lower signal and, thus, a lower amount of liquid.

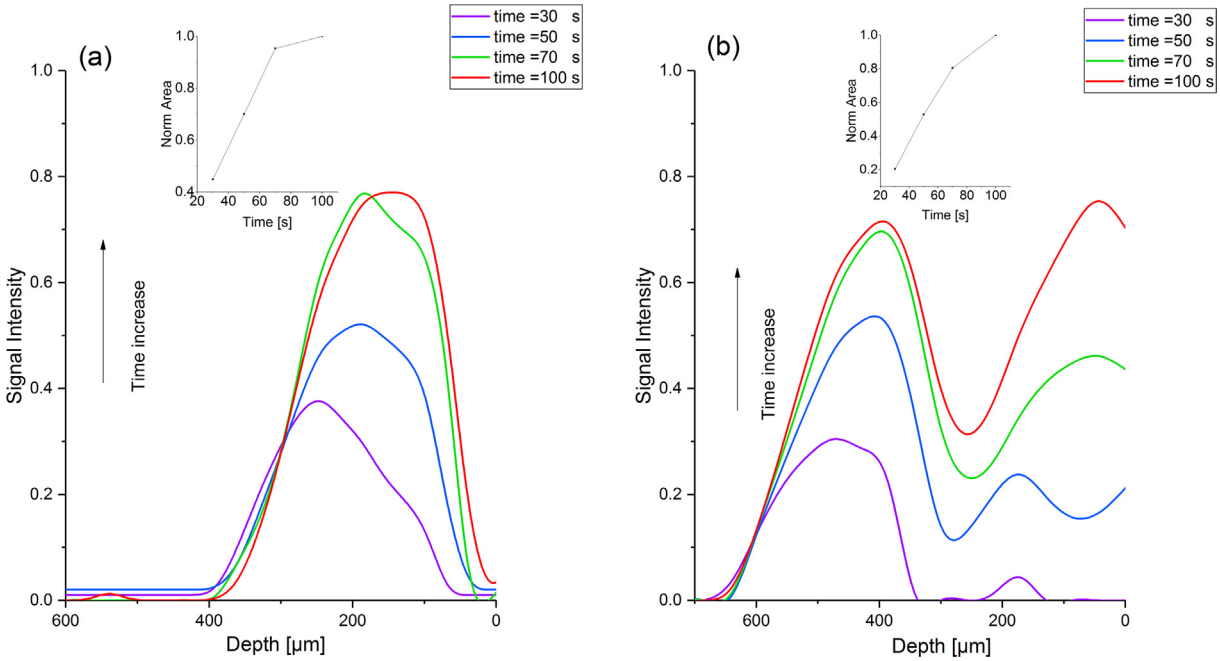

Fig. 6. The liquid distribution profiles after 30, 50, 70 and 100 s for (a) one single 86 gsm fibrous layer without an interface and (b) two 43 gsm fibrous layers with an interface. The zero position indicates the surface of the NMR sensor. The normalized areas below the curves versus time are shown in the insets.

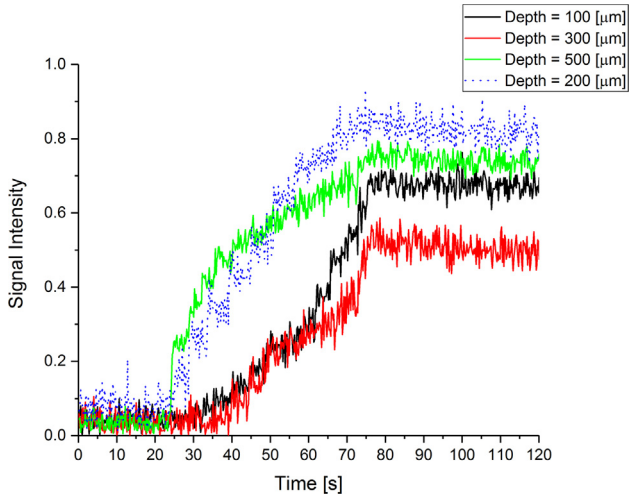

Fig. 7. The dynamic behavior of the fluid flow through one and two fibrous layers. The signal amplitudes over time are extracted at 100, 300 and 500 μm from the surface of the sensor which correspond to the positions of the second layer, interface area and first layer, respectively (solid lines). They are compared to the data obtained in the center of the single layer at 200 μm.

the sensor, which roughly correspond to the position of the second layer, the interface and the first layer, respectively. For the 400-μm single layer, the changes in signal intensity over time are obtained in the center of the layer i.e. 200 μm from the surface of the NMR sensor (dotted line in Fig. 7).

The slopes of the curves in Fig. 7 indicate the fluid flow velocity at each position. The simplest case is that of the 400-um single layer, where the dynamic curve (dotted line) has an almost constant slope until it reaches a constant plateau and equilibrium. The curve that illustrates the dynamic behavior of the top layer of a two-layer stack (green line) consists of a section with a steep slope followed by a part with a gentle slope. The point at which the slope changes corresponds to the time at which liquid starts to flow from the top layer into the interface area and the bottom layer.

The signal amplitude increases with the same slope, and thus the same speed, for both the interface region (red line) and the bottom layer (black line). However, after about 50 s, the slope in the interface region decreases. By comparing the slopes of these dynamic curves for the top and the bottom layers, one can conclude that liquid does not flow with the same speed through them.

The slopes of the dynamic curves were derived by taking the derivative of the curves and are shown in Fig. 8. The slope increases drastically as liquid infiltrates into the single layer and remains almost constant before it reaches zero at equilibrium (dotted line). The calculated time-dependent slope for the top layer of the two stacked layers (green line) consists of two parts: It starts with a higher value and decreases as velocity increases at the interface region (red line) and bottom layer (black line). The different dynamic behaviors of a single and a stack of two fibrous layers, reveals the importance of the interface affecting the fluid flow properties.

The relevance of interlayer pore space of thin fibrous layers in unsaturated fluid flow was discussed in our last study which was about liquid redistribution in the stack of two thin layers [27]. A coefficient used in the model for exchange of mass between those two layers was defined in a way to reproduce the delaying mechanism observed in experiments. The current study confirms the importance of the interface between two layers on unsaturated fluid flow qualitatively. As depicted in Figs. 3 and 7, the higher porosity and therefore lower capillarity of interlayer pore space changes the dynamic of fluid flow in a stack of two layers comparing to that of a single layer.

The temporal and dynamic data, together with the liquid distribution profiles, provide crucial experimental information to understand and model the effect of an interface on fluid flow through thin porous layers. These results could be included in simulations of flow in a stack of layers by modeling the interface as a virtual third layer or by defining an appropriate mass exchange coefficient with specific hydraulic properties.

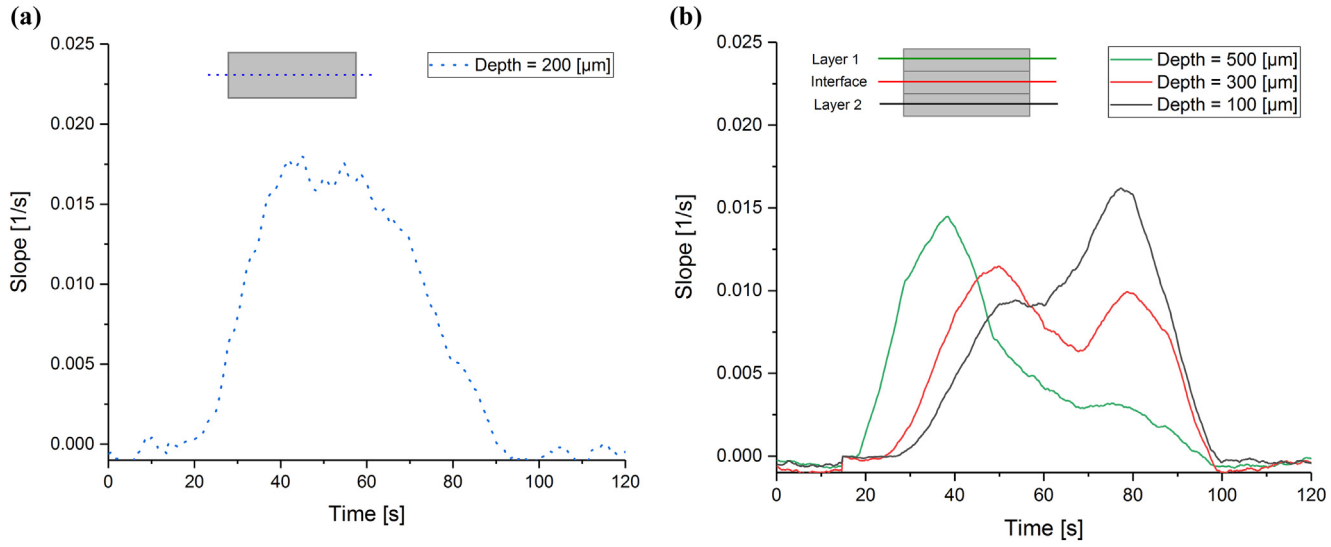

Fig. 8. The slope of intrusion curves which indicates velocity of liquid infiltration per time. The slope is extracted in the center of the single layer at 200 μm (a) and at 100, 300 and 500 μm from the surface of the sensor which correspond to the positions of the second layer, interface area and first layer, respectively (b).

5. Conclusion

This experimental study has applied the Fourier NMR-MOUSE – a novel, non-invasive method to explore and visualize the liquid flow in the interface regions of stacked thin fibrous layers. Employing a unique single-sided NMR sensor with a low but uniform static gradient has enabled us to acquire depth profiles across 2 mm in a single scan. To correct for measurement artifacts, the depth profiles measured for porous layers were normalized to those of pure water.

The influence of an interface region on the liquid flow has been clearly shown by comparing the dynamic responses as well as the liquid distribution profiles for a single fibrous layer and a stack of two fibrous layers. The slope increases drastically as liquid infiltrates into the single layer and remains almost constant before it reaches zero at equilibrium. The calculated time-dependent slope for the top layer of the two stacked layers comprises two parts, starting with a higher value and decreasing as velocity increases at the interface region and bottom layer. Thus, the different dynamic behaviors of a single fibrous layer and of a stack of two fibrous layers unmask the importance of the interface on fluid flow properties.

Ultimately, we have shown that the presence of an interface considerably affects the liquid flow across the thin layers. The results of this investigation will serve to validate numerical studies on fluid flow inside thin layers and through interfaces (such as [27]). The method of study presented in this work can be extended to multilayered porous media such as the proton exchange membranes fuel cells.

Acknowledgments

We are grateful to Uwe Mahla who helped us with taking the microscopy images of the thin layers.

References

[1] L. Ceballos, M. Prat, P. Duru, Slow invasion of a non-wetting fluid from multiple inlet sources in a thin porous layer, Phys. Rev. E 84 (2011) 056311.
[2] M. Prat, T. Agaësse, Thin Porous Media, in: K. Vafai (Ed.), Handbook of Porous Media (Chapter 4), third ed., Taylor & Francis, London, 2015.
[3] A.Z. Weber, J. Newman, Effects of microporous layers in polymer electrolyte fuel cells, J. Electrochem. Soc. 152 (2005) A677–A688.
[4] Z. Qi, A. Kaufman, Improvement of water management by a microporous sublayer for PEM fuel cells, J. Power Sources 109 (2002) 38–46.
[5] H.-J.G. Diersch, V. Clausnitzer, V. Myrnyy, R. Rosati, M. Schmidt, H. Beruda, B.J. Ehrnsperger, R. Virgilio, Modeling unsaturated flow in absorbent swelling porous media: Part 2. Numerical simulation, Transp. Porous Media 86 (2011) 753–776.
[6] A. D'Hueppe, M. Chandesris, D. Jamet, B. Goyeau, Coupling a two-temperature model and a one-temperature model at a fluid-porous interface, Int. J. Heat Mass Transf. 55 (2012) 2510–2538.
[7] D. Jamet, M. Chandesris, B. Goyeau, On the equivalence of the discontinuous one- and two-Domain Approaches for the modeling of transport phenomena at a fluid/porous interface, Transp. Porous Media 78 (3) (2009) 419–438.
[8] C.Z. Qin, S.M. Hassanizadeh, Multiphase flow through multilayers of thin porous media: general balance equations and constitutive relationships for a solid-gas-liquid three-phase system, Int. J. Heat Mass Transf. 70 (2014) 693–708.
[9] C.Z. Qin, S.M. Hassanizadeh, A new approach to modelling water flooding in a polymer electrolyte fuel cell, Int. J. Hydrogen Energy 40 (2015) 3348–3358.
[10] M. Weder, P.A. Bruhwiler, A. Laib, X-ray tomography measurements of the moisture distribution in multilayered clothing systems, Text. Res. J. 76 (2006).
[11] M. Weder, P.A. Bruhwiler, U. Herzig, R. Huber, G. Frei, E. Lehmann, Neutron radiography measurements of moisture distribution in multilayer clothing systems, Text. Res. J. 74 (2004) 685–700.
[12] J. Leisen, H.W. Beckham, Quantitative magnetic resonance imaging of fluid distribution and movement in textiles, Text. Res. J. 71 (2001) 1033–1045.
[13] J. Hoferer, M.J. Lehmann, E.H. Hardy, J. Meyer, G. Kasper, Highly resolved determination of structure and particle deposition in fibrous filters by MRI, Chem. Eng. Technol. 29 (2006) 816–819.
[14] M.J. Lehmann, E.H. Hardy, J. Meyer, G. Kasper, MRI as a key tool for understanding and modelling the filtration kinetics of fibrous media, Magn. Reson. Imag. 23 (2005) 341–342.
[15] J. Leisen, B. Hojjatie, D.W. Coffin, H.W. Beckham, In-plane moisture transport in paper detected by magnetic resonance imaging, Dry. Technol. 19 (2001) 199–206.
[16] J. Leisen, B. Hojjatie, D.W. Coffin, S.A. Lavrykov, B.V. Ramarao, H.W. Beckham, Through-plane diffusion of moisture in paper detected by magnetic resonance imaging, Indust. Eng. Chem. Res. 41 (2002) 6555–6565.
[17] J. Leisen, H.W. Beckham, Fluid distribution and movement in engineered fibrous substrates by magnetic resonance microscopy, Magn. Reson. Microsc.: Spatially Resolv. NMR Techniq. Applicat. (2009) 399–419.
[18] B. Blümich, F. Casanova, S. Appelt, NMR at low magnetic fields, Chem. Phys. Lett. 477 (2009) 231–240.
[19] B. Blümich, F. Casanova, M. Dabrowski, E. Danieli, L. Evertz, A. Haber, M. van Landeghem, S. Haber-Pohlmeier, A. Olaru, J. Perlo, O. Sucre, Small scale instrumentation for nuclear magnetic resonance of porous media, New J. Phys. 13 (2011) 1–15.
[20] B. Blümich, J. Perlo, F. Casanova, Mobile single-sided NMR, Prog. Nucl. Magn. Reson. Spect. 52 (2008) 197–269.
[21] J. Perlo, F. Casanova, B. Blümich, Profiles with microscopic resolution by single sided NMR, J. Magn. Reson. 176 (2005) 64–70.
[22] S. Rahmatallah, Y. Li, H.C. Seton, I.S. Mackenzie, J.S. Gregory, R.M. Aspden, NMR detection and one-dimensional imaging using the inhomogeneous magnetic field of a portable single-sided magnet, J. Magn. Reson. 173 (2005) 23–28.

[23] A.E. Marble, I.V. Mastikhin, B.G. Colpitts, B.J. Balcom, A constant gradient unilateral magnet for near-surface MRI profiling, J. Magn. Reson. 183 (2006) 228–234.
[24] Maxime Van Landeghem, Ernesto Danieli, Juan Perlo, Bernhard Blumich, Federico Casanova, Low-gradient single-sided NMR sensor for one-shot profiling of human skin, J. Magn. Reson. 215 (2012) 74–84.
[25] M.M. Tomadakis, S.V. Sotirchos, Ordinary and transition regime diffusion in random fiber structures, AIChE J. 39 (1993) 397–412.
[26] J. Whitcomb, X. Tang, Micromechanics of moisture diffusion in composite with impermeable fibers, J. Compos. Mater. 36 (2002) 1093–1101.
[27] A.H. Tavangarrad, B. Mohebbi, S.M. Hassanizadeh, R. Rosati, J. Clausen, B. Blümich, Continuum-scale modeling of liquid redistribution in a stack of thin hydrophilic fibrous layers, Transp. Porous Med. 122 (2018) 203–219, https://doi.org/10.1007/s11242-018-0999-0.